NANO LETTERS

2003
Vol. 3, No. 9
1293−1297

Tungsten Nitride Inverse Opals by Atomic Layer Deposition

Alessandro Rugge,[†] Jill S. Becker,[‡] Roy G. Gordon,*[,‡] and Sarah H. Tolbert*[,†]

Department of Chemistry and Biochemistry, University of California, Los Angeles, California 90095, and Department of Chemistry, Harvard University, Cambridge, Massachusetts 02138

Received May 30, 2003; Revised Manuscript Received June 23, 2003

ABSTRACT

In this letter, we demonstrate a new method of creating inverse opal structures by infiltrating thin-film colloidal crystals using atomic layer deposition (ALD) and then dissolving the templating particles. ALD offers several advantages over previous techniques including improved step-coverage of high aspect ratio structures and high conformality. In addition, ALD allows for the preparation of a large variety of non-oxide materials (in particular nitrides) with desirable optoelectronic properties and a diversity of phases. Here we form a metallic tungsten nitride inverse opal as an example.

Monodisperse colloidal particles are unique building blocks for materials displaying complex nanoscale structures. Arrays of submicrometer close-packed spheres with long-range order are easily grown from colloidal suspensions and may be used as templates for a diverse range of materials. The typical approach is to infiltrate the void space between the spheres of a colloidal crystal with the precursor(s) of the new material and to later remove the original particles later. This generates inverse opal structures whose size and chemical composition are tunable by the size of the colloids and the infiltration precursor(s), respectively. These structures have interesting potential applications as photonic materials because of the periodic variation of their dielectric constant and thus their potential to show a photonic band gap.[1−5]

A wide range of synthetic approaches have proved successful in creating inverse opal morphologies. Either latex or silica microspheres are typically used for the template because they are easy to prepare with narrow size distributions and with a wide range of precisely controlled submicrometer diameters. In addition, latex particles are easily eliminated by calcination, and silica colloids may be dissolved by etching with hydrofluoric acid. The two most common pioneering synthetic techniques[6] used to generate inverse opal structures were the hydrolysis of sol−gel precursors to yield inorganic oxides[7−12] and the polymerization of liquid monomers to yield several types of polymers.[12−16] Other techniques, including electroless and electrochemical deposition and nanocrystal infiltration, extended the possible range of materials to both metallic[12,17−19] and semiconducting[20,21] inverse opal structures. As the interest in this field grows, more approaches and synthetic variations have proved successful in the synthesis of inverse opal structures.[22] Chemical vapor deposition (CVD) is one of the more promising new techniques; it has been utilized to prepare carbon,[23] silicon,[24,25] and germanium[26] inverse opals. This technique can produce dense inverse opal structures by virtue of the gaseous precursor's ability to penetrate efficiently the pore network of colloidal crystals.

In this work, we report on the use of a new technique—atomic layer deposition (ALD)—to create inverse opals. ALD represents an innovative and very promising synthetic route to inverse opals because of its high degree of step coverage and conformality as well as its ability to grow dense films with good control of atomic structures. Perhaps most importantly, ALD is a chemically versatile technique that affords great control over the chemical composition of the inverse opal material templated from colloidal crystal arrays. If the potential of inverse opals to produce 3D photonic band gap structures is to be exploited, then the ability to choose materials with specific optical properties represents a key advantage of ALD relative to other infiltration techniques.

In this study, we present results on the ALD of tungsten nitride, WN, inside thin-film silica colloidal crystals that had been deposited on glass slides. Tungsten nitride was chosen for this study because it has been shown to form highly conformal coatings in structures with high aspect ratios.[27] In addition, WN is highly stable and is inert to hydrofluoric acid, which is used to remove the templating silica particles in the second step of the synthesis process. Furthermore, because of the metallic character of WN, imaging the resulting structure by scanning electron microscopy (SEM, Hitachi S4700) is straightforward. Direct imaging allowed

* Corresponding authors. E-mail: tolbert@chem.ucla.edu, gordon@chemistry.harvard.edu.
[†] University of California.
[‡] Harvard University.

10.1021/nl034362r CCC: $25.00
Published on Web 07/31/2003

us to examine the final morphology and understand how the ALD precursors infiltrate the templating opal. The opals were grown on thin glass slides so that after infiltration they could be released with HF, allowing us to examine both the top and bottom surfaces of the film.

Silica particles were prepared by the Stöber method with the following modifications.[28] Tetraethoxyorthosilicate (TEOS) was hydrolyzed by small amounts of water in an ethanolic solution in the presence of ammonia. The reagents were mixed and stirred in a sealed plastic container for at least 3 h at room temperature. The amount of water and ammonia present in solution regulates the rates of nucleation and growth for the particles and ultimately affects their size. The particle population used in this study had an average diameter of 298 nm $\pm$ 2% and was purified by several cycles of centrifugation and resuspension in absolute ethanol. Calculations of size and size distribution for the population were obtained from the purified products by measuring the size of at least 100 particles in transmission electron microscopy (TEM) images.

The colloidal crystals were prepared by an established vertical deposition technique.[29,30] A thin glass slide was held vertically in a 20-mL vial containing an ethanol suspension of 0.25 to 1.0 vol % particles. As the ethanol evaporates and the meniscus sweeps down the substrate, capillary forces induce an ordering of the particles into a close-packed arrangement. Films were typically grown at a rate of 5 to 6 mm/day. For this study, we prepared opal films with thickness ranging from 1.5 to 15 μm. This technique produces multilayered close-packed colloidal crystals that are firmly attached to the substrate with the (111) planes of the colloidal array parallel to the substrate. As the films dry and possibly shrink, however, the large crystalline domains tend to crack. This generates a collection of irregularly shaped islands ranging from a few to several hundred micrometers in size. These islands are separated by a network of deep fractures perpendicular to the substrate that can be up to 2 μm wide.

Atomic layer deposition is a process for depositing thin layers of solid materials from two or more vapor precursors.[31] The surface or template onto which the film is to be deposited is exposed to a dose of vapor from one precursor until it becomes saturated with up to one monolayer of coverage. Any excess unreacted vapor from that precursor is then pumped away. Next, a vapor dose from the second precursor is brought to the surface and allowed to react to reactivate the surface toward the first precursor. This cycle of steps can be repeated to build up thicker films. One particularly important aspect of this process is that the ALD reactions are self-limiting in that only a certain maximum thickness can form in each cycle, even if excess reactant is available. Because of this self-limiting character, ALD reactions produce coatings with highly uniform thicknesses not only on flat surfaces but also inside narrow holes and trenches. In this work, we show that this process is also suitable for the infiltration of the interconnected porous network between the spheres of a colloidal crystal by growing a conformal film on the surface of all colloids.

WN was grown within the colloidal crystal substrates using specially designed equipment and optimized procedures that have been described elsewhere.[27] In the case of tungsten nitride films, the precursor gases being cycled through the deposition chamber were bis(*tert*-butylimido)bis-(dimethylamido)tungsten(VI) and ammonia. In the original studies, the growth of WN films on flat substrates never exceeded 0.1 nm/cycle at 350 °C because of the self-limiting nature of the reactions involved. The fact that a very thin layer is deposited during each cycle is of great importance if as much of the porosity of the opal as possible is to be filled with WN before access to the inner spaces between the spheres is blocked off.

After infiltration, the substrates were soaked in 5−10% HF for several hours. Whereas the silica particles are dissolved within minutes by HF under these conditions, the longer soak allowed us to dissolve the thin glass slide that the colloidal crystal was originally grown on as well. The resulting macroscopic flakes of inverse opal films could be handled with tweezers. This material was then deposited onto a silicon substrate for SEM imaging.

Figure 1 shows examples of typical inverse opal structures achievable by ALD. The sample that is shown was infiltrated with a dose of tungsten precursor of 1.3 μmol/cycle, followed by a dose of ammonia of 1.8 mmol/cycle. These amounts correspond to exposures of 1.1×10^5 and 4.2×10^7 Langmuirs (1 Langmuir $= 10^{-6}$ Torr s) of tungsten precursor and ammonia, respectively. More specifically, the dose of tungsten precursors delivered to the substrate per unit area (as estimated by adding the surface area of the deposition chamber and the internal surface area of the colloidal array) was $\sim$2.6 nmol/cm^2. These conditions achieved infiltration of WN throughout the opal structure.

A view of a step of an infiltrated colloidal crystal is shown before (Figure 1a) and after (Figure 1b) the removal of the close-packed silica particles. The gaseous precursors enter the interconnected porous network formed by the microspheres from the top surface and sides of the colloidal crystal. As mentioned earlier, the cracks between the islands that form during the drying of the colloidal film turn out to be another major route to the deeper layers of particles near the glass substrate. Figure 1c shows the bottom surface of the inverse opal after the dissolution of the surrounding silica particles and of the glass slide that it was in contact with. The hexagonally arranged dark holes represent the points where the bottom monolayer of silica particles was in contact with the substrate. The fact that the space between these points of contact appears flat and filled with WN is proof that the infiltration of the colloidal crystal is complete all the way down to the substrate.

By varying the ALD deposition conditions, we can learn about the infiltration mechanism and learn what conditions most effectively optimize infiltration. To identify failure mechanisms for ALD as an opal infiltration technique, we markedly decreased the dose of tungsten precursor by a factor of 16 from 1.3 μmol to 81 nmol/cycle, corresponding to an exposure of only 6.9×10^3 Langmuirs. The same ammonia dose of 1.8 mmol/cycle was used because this reagent was always present in large excess relative to the tungsten precursor.

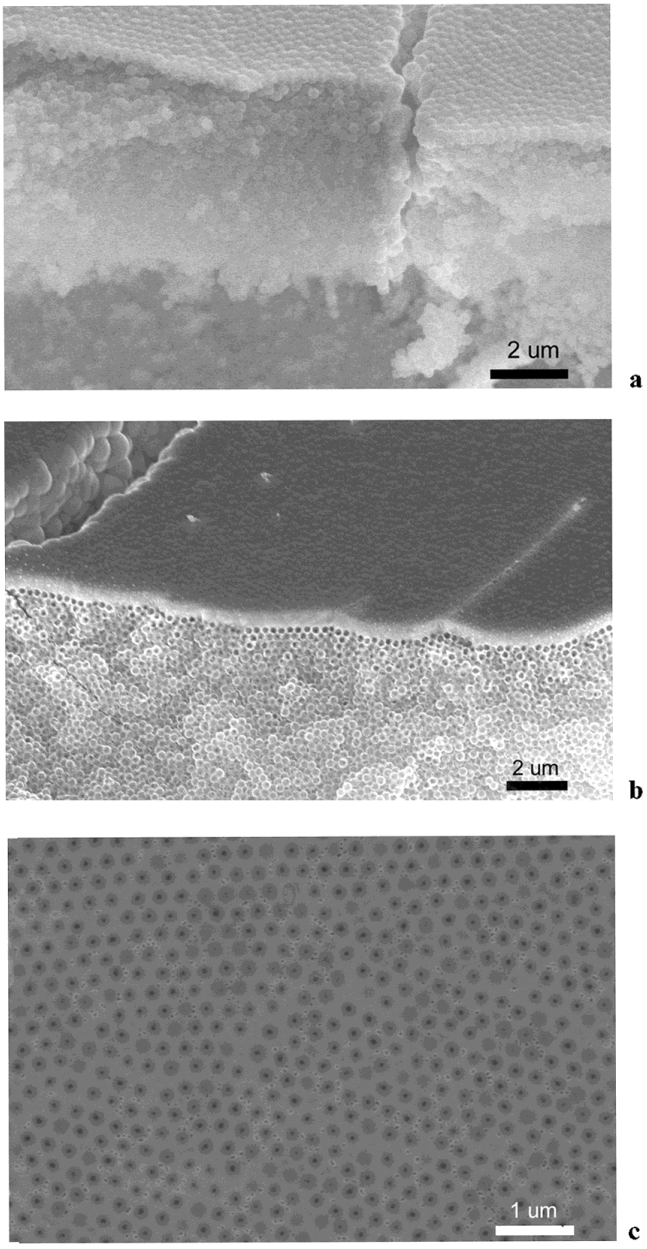

Figure 1. (a) Colloidal crystal film infiltrated with WN. Conformal growth of the nitride is apparent on the top surface of the film, but colloids deep within the film can grow only until the access of the gas precursor is blocked. (b) Same inverse opal structure obtained after the silica particles are dissolved. (c) Bottom surface of the inverse opal after removing the substrate. The hexagonal array of holes corresponds to the points of contact between the first monolayer of particles and the glass substrate, which proves that the infiltration is complete down to the substrate.

Although these conditions are sufficient to grow a 100-nm-thick film of WN on a flat substrate at 350 °C (0.1 nm/cycle growth), they resulted in incomplete infiltration of the opal layer. The incomplete infiltration pattern obtained when using these underdosing conditions is apparent in the sample shown in Figure 2. The sample appears to consist of many islands, and each island is infiltrated from its top surface as well as from the cracks that separate it from the surrounding islands. This is clear when an unetched film is scraped off of the substrate and the footprints of the infiltration patterns

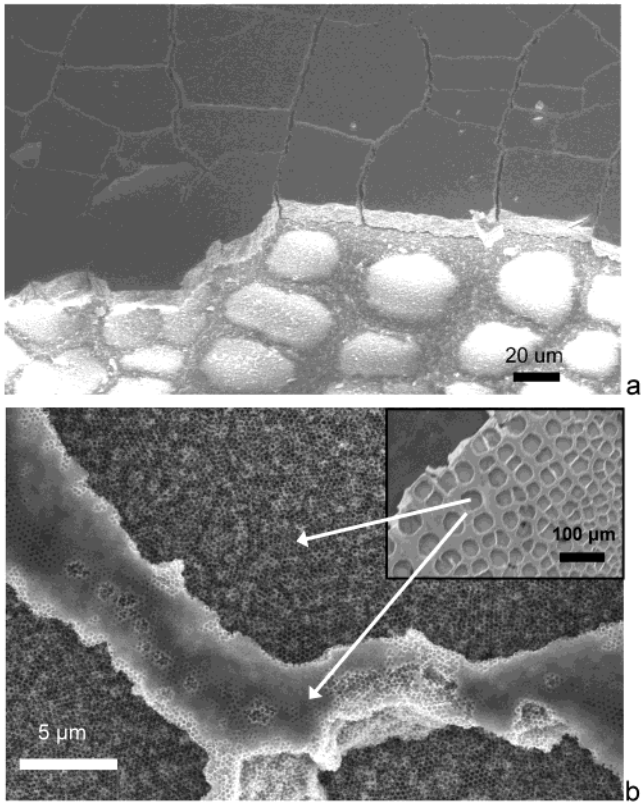

Figure 2. (a) Several islands of a partially infiltrated colloidal crystal film before etching of the colloids. The round, light areas in the foreground correspond to portions of the substrate not reached by WN during the deposition process. (b) Low- (inset) and high- (main panel) resolution images of the bottom surface of the partially filled array after dissolving the silica. The cavities in the inset are formed from the uninfiltrated portions at the center of the islands and correspond to the light footprints in part a. The main panel shows that WN inverse opal structures extend down to the substrate in the proximity of the cracks separating two islands. The darker inverse opal structure in the background is the result of infiltration only from the top surface of the island.

are imaged (Figure 2a). The light areas arranged with a pattern similar to the islands of colloidal crystals correspond to the interior portions of the opal that have not been reached by the gaseous precursors. When the silica is dissolved and the bottom surface of the inverse opal is imaged (Figure 2b), those same areas now appear as large cavities. Apparently, the gaseous precursors did not penetrate the opal all the way to the glass substrate. As the gases diffuse into the network, they react with the first surfaces they contact. The reactive precursors are thus depleted before they can travel to colloid surfaces buried deep within the colloidal array. In other words, under these underdosing conditions, the amount of precursor vapor that the opal is exposed to is not sufficient to coat the entire internal surface, leaving only the more easily accessible surfaces coated and large portions of the inner colloidal crystal unaltered.

Once optimal dosage conditions were established, we could then begin to explore morphology. After the dissolution of the silica template in fully dosed samples, the details of the inverse opal film were imaged at high resolution to assess the potential of this technique to produce materials for photonic applications (Figure 3). The main morphological

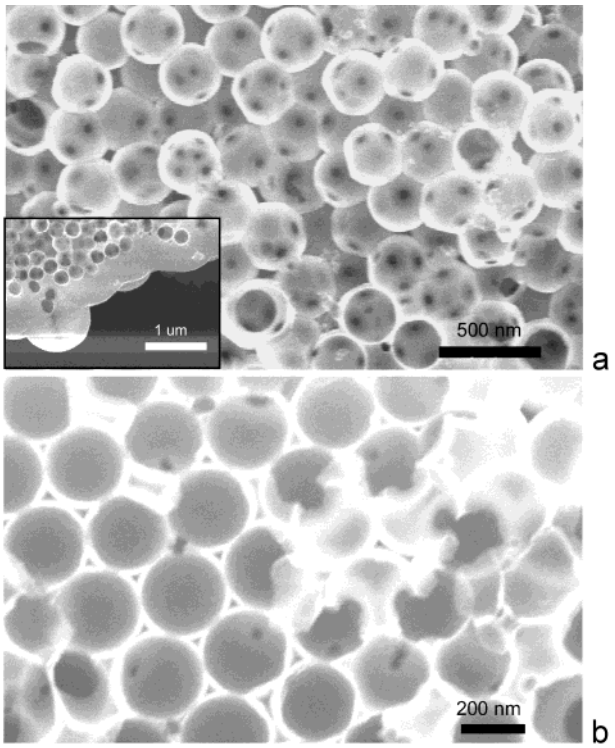

Figure 3. Typical morphological features of a WN inverse opal. (a) WN spherical shells are the main morphological feature observed in these systems. The dark holes represent the point of contact between each templating sphere and its 12 nearest neighbors. The inset shows a portion of a surface of the inverse opal structure displaying a conformal overlayer and a thin underlying region characterized by completely filled interstices. (b) Cross section of the spherical shells showing the thickness of the shells and the size of the tetrahedral pores between spheres.

feature observed for fully infiltrated opals such as the one shown in Figure 1 is an array of close-packed WN spherical shells. Each shell displays 12 regularly arranged small holes measuring about 30−35 nm in diameter (Figure 3a). These holes correspond to the touching points between each templating sphere and its nearest neighbors, which are regions that could not be filled with WN. These small holes also provide the connections that are required to dissolve the silica particles with a wet etch.

Figure 3b shows an example of cross sections of close-packed spherical shells such as the ones from Figure 3a. The shells have a thickness of approximately 20 nm. The spherical holes measured in the inverse opal structure have an average diameter of about 250 nm. This value is significantly smaller than the 298-nm diameter measured by TEM on the original particles. We believe the shrinkage of the particles to be caused by heating the templating colloidal crystal in the ALD apparatus to 350 °C. This is expected to sinter the opal and to favor the formation of necks between nearest-neighbor particles, resulting in the 30−35 nm holes mentioned above. Each cluster of four adjacent spherical shells encloses a tetrahedral pore in the inverse opal structure. This cavity is sealed when the thickness of WN shells templated on the spheres exceeds a threshold value and blocks the access of the precursors to the tetrahedral cavities. It should be noted that this spherical shell morphology was shown to be an optimal structure for photonic applications because the width of the band gap in these systems is calculated to be significantly larger than the structure with no tetrahedral pores between each cluster of four air spheres.[2,25] ALD should thus allow us to maximize the width of the stop band by precisely controlling the thickness of the spherical shells with the number of deposition cycles.

The inset in Figure 3a shows an example of the morphology observed at the top surface of the resulting inverse opal structure. The top surface (as well as the vertical walls on each side of a crack separating two islands) is typically covered with a thick overlayer of solid WN. This overlayer thickness can be controlled by optimizing the deposition conditions. As the deposited material grows conformally on the outer faces of these spheres, the surface features are "magnified" at each deposition step. The results suggest that an optimized protocol for the infiltration of opals requires the minimum number of high-exposure cycles needed to reach a point where the pores are blocked off but no significant overlayer has an opportunity to grow. Immediately below the overlayer, we observed a region a few particle diameters thick characterized by complete infiltration of the porosity with solid WN (Figure 3a, inset). The added porosity of the top surface probably allows for complete filling of the interstitial spaces for the first one or two particle layers.

As mentioned earlier, one of the major advantages of ALD compared to other gas-phase deposition techniques is its self-limiting growth mechanism and thus its ability to infiltrate deep pores. To tune the deposition conditions for thicker films, we must consider the atomic details of the ALD process. In the first place, the dose of precursor vapor required to saturate the surface area of the colloidal crystal should increase linearly with its thickness. The exact dose that is required depends on the area of the deposition chamber and on the surface area of the particles in the opal, which may be estimated from the size of the colloidal crystal, the number of particle layers, and the average diameter of the component particles. In the case of holes and trenches such as the tortuous porous network inside colloidal crystals, diffusion models predict that the exposure time to each precursor required for conformal coverage also increases linearly with the colloidal crystal thickness.[32] Therefore, the exposure (precursor vapor partial pressure multiplied by the time the vapor is exposed to the substrate) required for conformal coverage of the internal surface area of the colloids crystal is predicted to increase with the square of the number of particle layers. In this study, we have been able to achieve complete infiltration for colloidal crystal films up to about 15 μm in thickness. Even larger thicknesses could be infiltrated by providing a valve between the deposition chamber and the vacuum pump. In this way, the reactive vapors can be exposed to the substrate for a longer time than in the present experiments, in which the vapors passed quickly (in about 0.2 s) through the deposition chamber.

The atomic structure of WN templated on colloidal crystals at 350 °C appears to be partially crystalline as deposited (Figure 4a). The atomic order may be improved by heating the inverse opal (after removing the silica) at 600 °C for 2 h

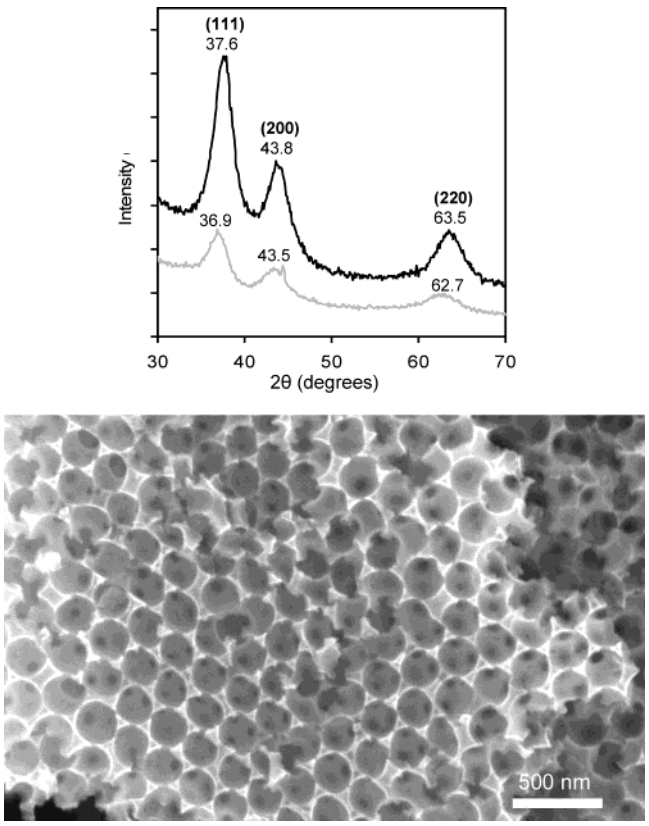

Figure 4. (a) X-ray diffraction patterns of inverse opals as-prepared (grey) and after annealing at 600°C for 2 h (black). The atomic-scale order increases and the lattice spacings reach the values reported for bulk WN. (b) After heating, the inverse opal architecture remains intact.

without damaging the inverse opal morphology (Figure 4b). Heating the samples to 700 °C resulted in the decomposition of WN to tungsten metal and in the collapse of the inverse opal structure. The size of the crystalline domains estimated from the width of the X-ray diffraction (XRD) peaks was 3.5 to 4 nm for both the as-prepared and heated samples.

In summary, this work shows that atomic layer deposition is a powerful new synthetic route for preparing inverse opals templated by colloidal crystals. By using sufficiently high exposures of precursors, relative to the surface area of the colloidal crystals, fully infiltrated substrates can be produced for opal films with thicknesses up to 15 μm. Dissolution of the templating silica particles produces an inverse opal structure composed of close-packed spherical shells of WN. The crystallinity of WN can be improved with heating without damaging the inverse opal architecture.

We have chosen WN as a proof-of-concept material in this work because of its favorable properties described above. However, the great chemical versatility of ALD should allow for the preparation of inverse opals from a wide range of materials for many different applications. Inverse opals, although porous and lightweight, are robust structures that can find useful applications in many fields depending on the optoelectronic properties of the framework. The great chemical versatility of ALD makes it possible to obtain materials with different band gaps and dielectric properties. The ability to control the thickness of the spherical shells making up the inverse opal architecture is ideal for photonic band gap applications.[2,25] In addition, inverse opal structures obtained by ALD may be further modified by filling the empty spaces originally occupied by silica particles (by means of ALD processing or other techniques) to generate a large variety of composite materials that couple the properties of two or more specifically chosen components.

Acknowledgment. This work was supported by the Office of Naval Research under grant N00014-99-1-0568 (S.H.T.) and by the National Science Foundation under grant ECS 9975504 (R.G.G.). S.H.T. is an Alfred P. Sloan Foundation Research Fellow.

References

(1) Yablonovitch, E. *J. Opt. Soc. Am. B* **1993**, *10*, 283. Yablonovitch, E.; Gmitter, T. L. *Phys Rev. Lett.* **1989**, *63*, 1950.
(2) Busch, K.; Sajeev, J. *Phys. Rev. E* **1998**, *58*, 3896.
(3) Ho, K. M.; Chan, C. T.; Soukoulis, C. M. *Phys. Rev. Lett.* **1990**, *65*, 3152
(4) Biswas, R.; Sigalas, M. M.; Subramania, G.; Ho, K. M. *Phys. Rev. B* **1998**, *57*, 3701.
(5) Moroz, A.; Sommers, C. *J. Phys.: Condens. Matter* **1999**, *11*, 997.
(6) Velev, O. D.; Kaler, E. W. *Adv. Mater.* **2000**, *12*, 531.
(7) Imhof, A.; Pine, D. J. *Nature* **1997**, *389*, 948.
(8) Holland, B. T.; Blanford, C. F.; Stein, A. *Science* **1998**, *281*, 538. Holland, B. T.; Blanford, C. F.; Do, T.; Stein, A. *Chem. Mater.* **1999**, *11*, 795. Holland, B. T.; Abrams, L.; Stein, A. *J. Am. Chem. Soc.* **1999**, *121*, 4308.
(9) Wijnhoven, J. E. G.; Vos, W. L. *Science* **1998**, *281*, 802.
(10) Yin, J. S.; Wang, Z. L. *Adv. Mater.* **1999**, *11*, 469.
(11) Yang, P. D.; Deng, T.; Zhao, D. Y.; Feng, P. Y.; Pine, D.; Chmelka, B. F.; Whitesides, G. M.; Stucky, G. D. *Science* **1998**, *282*, 2244.
(12) Jiang, P.; Bertone, J. F., Colvin, V. L. *Science* **2001**, 291, 453.
(13) Park, S. H.; Xia, Y. N. *Chem. Mater.* **1998**, *10*, 1745. Park, S. H.; Xia, Y. N. *Adv. Mater.* **1998**, *10*, 1045.
(14) Gates, B.; Yin, Y.; Xia, Y. N. *Chem. Mater.* **1999**, *11*, 2827.
(15) Johnson, S. A.; Ollivier, P. J.; Mallouk, T. E. *Science* **1999**, *283*, 963.
(16) Jiang, P.; Cizeron, J.; Bertone, J. F.; Colvin, V. L. *J. Am. Chem. Soc.* **1999**, *121*, 11 630.
(17) Yan, H. W.; Blanford, C. F.; Holland, B. T.; Parent, M.; Smyrl, W. H.; Stein, A. *Adv. Mater.* **1999**, *11*, 1003.
(18) Velev, O. D.; Tessier, P. M.; Lenhoff, A. M.; Kaler, A. M. *Nature* **1999**, *401*, 548.
(19) Jiang, P.; Cizeron, J.; Bertone, J. F.; Colvin, V. L. *J. Am Chem. Soc.* **1999**, *121*, 7957.
(20) Vlaslov, Y. A.; Bo X.-Z.; Sturm, J. C.; Norris, D. J. *Science* **2001**, *414*, 289.
(21) Braun, P. V.; Wiltzius, P. *Nature* **1999**, *402*, 603.
(22) Many examples are included in the special issue *Adv. Mater.* **2001**, *13*(6).
(23) Zakhidov, A. A.; Baughman, R. H.; Iqbal, Z.; Cui, C.; Khayrullin, I.; Dantas, S. O.; Marti, J.; Ralchenko, V. G. *Science* **1998**, *282*, 897.
(24) Vlaslov, Y. A.; Bo X.-Z.; Sturm, J. C.; Norris, D. J. *Science* **2001**, *414*, 289.
(25) Miguez, H.; Tetreault, N.; Yang, S. M.; Kitaev, V.; Ozin, G. A. *Adv. Mater.* **2003**, *15*, 597.
(26) Meseguer, F.; Blanco, A.; Miguez, H.; Garcia-Santamaria, F.; Ibisate, M.; Lopez, C. *Colloids Surf.* **2002**, *202*, 281.
(27) Becker, J. S.; Gordon, R. G. *Appl. Phys. Lett.* **2003**, *82*, 2239. Becker, J. S.; Suh, S.; Gordon, R. G. *Chem. Mater.*, ASAP Article, Web Release Date: June 20, 2003.
(28) Bogush, G. H.; Tracy, M. A.; Zukoski IV, C. F. *J. Non-Cryst. Solids* **1988**, *104*, 95.
(29) Dimitrov, A. S.; Nagayama, K. *Langmuir* **1996**, *12*, 1303.
(30) Jiang, P.; Bertone, J. F.; Hwang, K. S.; Colvin, V. L. *Chem. Mater.* **1999**, *11*, 2132.
(31) Ritala, M.; Leskelä, M. Deposition and Processing. In *Handbook of Thin Film Materials*; Nalwa, H. S., Ed.; Academic Press: San Diego, CA, 2002; Vol. 1, p 103.
(32) Gordon, R. G.; Hausmann, D.; Kim, E.; Shephard, J. *Chem. Vap. Deposition* **2003**, *9*, 73.

NL034362R